Finite Element Simulation of Mechanical Behavior of TRIP800 Steel Under Different Loading Conditions Using an Advanced Microstructure-Based Model

F. HOSSEINABADI, A. REZAEE-BAZZAZ, and M. MAZINANI

The mechanical behavior of a low alloy multiphase TRIP steel has been predicted by an advanced microstructure-based finite element method. A representative volume element chosen based on the actual microstructure has been utilized for simulating the mechanical behavior of the studied steel. The parameters describing the martensitic transformation kinetics have been estimated using both crystallographic and thermodynamic theories of martensitic transformation. The mechanical behavior of each of the constituent phases required for the prediction of mechanical behavior of the studied material has been extracted from those reported in the literature. Comparison of the predicted mechanical behavior of the investigated TRIP800 steel with those reported in the literature shows that there is good agreement between simulated and experimental results. Therefore, it can be said that, the utilized microstructure-based model can be used for the prediction of both mechanical and transformation behaviors of the TRIP800 steels. It is worth noting that all of the parameters used in the model, except the sensitivity of the martensitic transformation to the stress state, can be estimated theoretically; thus, the number of parameters obtained by correlating the simulated and experimental results reduces to one. This is the unique characteristic of the utilized model, which makes the application of the model for simulation of the mechanical behavior of TRIP steels simpler than that of the similar ones.

DOI: 10.1007/s11661-016-3879-7

I. INTRODUCTION

LOW-ALLOYED TRIP steels are known as an important class of low alloy high-strength (HSLA) steels with a multiphase microstructure consisting of bainite and retained austenite within the ferrite matrix. Desirable combination of high strength and good ductility of TRIP steels is mainly due to the occurrence of strain-induced martensitic transformation of metastable-retained austenite.[1] Because of this suitable combination of strength and ductility, application of TRIP steels may lead to an improved crash worthiness accompanied by weight reduction in automotive industries.

During the last three decades, a number of considerable attempts have been made for simulating the deformation behavior of TRIP steels on the macroscopic level.[2–8] One of the first research works with regard to this research topic has been carried out by Olson and Cohen[2] in which a physical-based model has been developed for predicting temperature-dependent strain-induced martensitic transformation in TRIP steels. The next attempts were focused on generalization of Olson and Cohen's model through which the effect of mechanical driving force on martensitic transformation was studied by Stringfellow *et al.*[3] The subsequent series of investigations on the basis of the model proposed by Olson and Cohen have been done by incorporating the stress state and austenite grain size effects on the transformation of martensite.[4,5] The effects of hardening behavior, composition, and morphology of the constituent phases on overall mechanical behavior of TRIP steels have been also considered using physical and numerical models.[6–8]

The mechanical properties of multiphase TRIP steels are strongly dependent upon their composite-type microstructures. Therefore, estimation of these properties in microscopic level needs to be taken into account. Several micromechanics-based models have been introduced and exploited to simulate local deformation behavior of multiphase TRIP steels.[9–12] Marketz and Fischer[9] performed a micromechanical study in order to predict micro-stress and micro-strain distributions within and around the plate-shaped martensitic variants. Riesnert *et al.*[10] proposed a transformation criterion on the basis of thermodynamics for predicting the onset of the strain-induced martensitic transformation and/or its kinetics and suggested that the stability of austenite phase against strain-induced martensitic transformation shows marked load-type sensitivity. Taleb and Sidoroff[11] applied the micromechanical model of Green wood–Johnson mechanism for simulation of transformation-induced plasticity and improved the model's prediction by modifying some of the presumptions. Han *et al.*[12] developed a microstructure-based computational model in which the martensitic transformation

F. HOSSEINABADI, A. REZAEE-BAZZAZ, and M. MAZINANI are with the Department of Metallurgy and Materials Engineering, Faculty of Engineering Ferdowsi University of Mashhad, Mashhad, Iran. Contact e-mail: bazaz-r@um.ac.ir
Manuscript submitted February 28, 2016.
Article published online November 28, 2016

kinetics was assumed to be a nucleation-controlled phenomenon and predicted the change of M_s temperature under different loading conditions.

In most of the previous studies, simple representative volume elements (RVE's) have been used in the finite element simulation for considering the effect of microstructure on the mechanical properties of TRIP steels. In recently conducted investigations, however, the representative volume elements based on the real microstructure have been utilized to estimate the mechanical properties of multiphase TRIP steels.[13–15] Choi *et al*. have predicted the change of austenite volume fraction in a commercial TRIP800 steel sheet during straining and then, estimated its engineering stress–strain curve by the use of the representative volume element developed based on its real microstructure obtained by scanning electron microscope. The mechanical behavior of constituent phases and the fitting parameters describing the martensite transformation kinetics were determined using the high-energy X-ray diffraction experiment. A good correlation was found between the overall macroscopic behavior of the steel and that estimated by the computed response of the representative volume element.[13]

The microstructure-based finite element model used for estimating engineering stress–strain curve of the commercial TRIP800 steel has been also utilized for predicting its ductility and failure mode, and acceptable agreement has been found between the experimental and predicted results.[14] In another research, the microstructure-based finite element model used in two previous investigations has been applied as a virtual design tool in investigating the influence of various materials design parameters on the deformation behavior of TRIP steels.[15]

In the investigations performed by Choi and his coworkers, a stress invariant-based transformation kinetics law has been used in order to capture the kinetics of martensitic phase transformation during deformation. The stress invariant transformation equation contains four parameters which should be determined for the prediction of overall deformation behavior of TRIP steel. Most of these constants are considered by Choi *et al*. to be the adjusting parameters, although they have particular physical meanings and therefore, it seems that they are calculable at a priori. The aim of the present study is to investigate the possibility of predicting overall deformation behavior of a low alloy TRIP steel using the transformation equation proposed by Choi *et al*. with the theoretically calculated parameters. This is novel and to the authors' knowledge, has not been attempted so far.

II. KINETICS OF MARTENSITIC PHASE TRANSFORMATION

The procedure used in recently conducted studies for micromechanical simulation of the TRIP800 steel based on its real microstructure[13–15] has been adopted in this work for the prediction of the mechanical behavior of a similar TRIP steel. The equations utilized for predicting the martensitic transformation kinetics together with theoretical parameters calculation method are briefly described in this section.

The martensitic domain formation is possible whenever the associated driving force reaches the critical energy barrier of the transformation.[16] Following Serri and Cherkaoui,[16,17] the macroscopic mechanical driving force for the martensitic transformation expressed as the following equation, has been utilized in the present study for predicting the transformation kinetics:

$$\overline{\sigma}^{A} : \tilde{\varepsilon}^{tr} = R\sqrt{3J_2}\left[1 + k\frac{J_3}{J_2^{3/2}}\right] + \frac{\alpha I_1}{3} \qquad [1]$$

where $\overline{\sigma}^{A}$ is the average stress in the austenite phase, $\tilde{\varepsilon}^{tr}$ denotes the average transformation strain, R corresponds to the maximum transformation shear strain, k described the sensitivity of the transformation to the stress state, and α is the volume strain accompanied by the martensitic transformation.

In Eq. [1], I_1 is the first invariant of stress tensor; J_2 and J_3 are the second and third invariants of deviatoric stress tensor, respectively.

The values of parameters R and α in Eq. [1] can be calculated based on the crystallographic description of martensitic transformation stated in References 18 and 19.

In ferrous alloys and during martensitic transformation, the FCC crystal structure of the parent phase changes into BCT structure of the product. The Bain strain, which corresponds to the transformation of a unit cell in the parent crystal structure into the product with the smallest atomic displacement, can be obtained as follows[18,19]:

$$(\gamma B \gamma) = \begin{pmatrix} \eta_1 & 0 & 0 \\ 0 & \eta_2 & 0 \\ 0 & 0 & \eta_3 \end{pmatrix}, \qquad [2]$$

where $\eta_1 = \eta_2 = \sqrt{2}\left(\frac{a_{\gamma'}}{a_\gamma}\right)$ and $\eta_3 = \frac{c_{\gamma'}}{a_\gamma}$. The subscripts γ and α' denote the austenite and martensite phases, respectively.

It has been shown that the invariant line of the martensitic transformation strain should be on the {110} planes of the austenite phase which do not contain the c axis of the martensite.[20] Considering one of these planes, the plane defined by the invariant—normal of the transformation strain should contain one of $\langle 1 \quad \bar{1} \quad 1 \rangle$ directions. Therefore, (101) and $[1 \quad 0 \quad \bar{1}]$ can be considered to be the plane containing the invariant line and direction lying on the invariant—normal plane of the transformation strain, respectively.

Considering the invariant line to be $[u_1 \quad u_2 \quad u_3]$, the vector $[u_1 \quad u_2 \quad u_3]$ will be on the plane $(1 \quad 0 \quad 1)$ when

$$u_1 = -u_3. \qquad [3]$$

Supposing $[u_1 \quad u_2 \quad u_3]$ to be a unit vector, then

$$u_1^2 + u_2^2 + u_3^2 = 1. \quad [4]$$

This vector changes into a new vector $[v_1 \quad v_2 \quad v_3]$ as a result of the Bain transformation using the following equation:

$$[v_1 \quad v_2 \quad v_3] = [u_1 \quad u_2 \quad u_3](\gamma B\gamma). \quad [5]$$

Since $[u_1 \quad u_2 \quad u_3]$ has been considered to be an invariant vector, its length should be unchanged after the Bain deformation. Therefore,

$$v_1^2 + v_2^2 + v_3^2 = u_1^2 + u_2^2 + u_3^2. \quad [6]$$

Solving Eqs. [3], [4], and [6] simultaneously, the indices of both the $[u_1 \quad u_2 \quad u_3]$ and $[v_1 \quad v_2 \quad v_3]$vectors will be calculated.

Similarly, the invariant unit vector perpendicular to the invariant line, *i.e.*, $[h_1 \quad h_2 \quad h_3]$ vector, can be calculated using the following equation resulting from the assumption that the plane indicated by $(h_1 \quad h_2 \quad h_3)$ contains $[1 \quad 0 \quad \bar{1}]$ direction.

$$h_1 = h_3 \quad [7]$$

This direction becomes the new vector$[l_1 \quad l_2 \quad l_3]$, because of the Bain deformation. Therefore,

$$[l_1 \quad l_2 \quad l_3] = [h_1 \quad h_2 \quad h_3](\gamma B\gamma)^{-1} \quad [8]$$

The invariance of $[h_1 \quad h_2 \quad h_3]$ vector requires that

$$l_1^2 + l_2^2 + l_3^2 = h_1^2 + h_2^2 + h_3^2. \quad [9]$$

Solving Eqs. [8] and [9] simultaneously and considering that the $[h_1 \quad h_2 \quad h_3]$ is a unit vector, the indices of both the $[h_1 \quad h_2 \quad h_3]$ and $[l_1 \quad l_2 \quad l_3]$ vectors are calculated.

One way for converting $(\gamma B\gamma)$into an invariant line strain is to employ a rigid body rotation which simultaneously rotates $[l_1 \quad l_2 \quad l_3]$ into $[h_1 \quad h_2 \quad h_3]$ and $[v_1 \quad v_2 \quad v_3]$ into $[u_1 \quad u_2 \quad u_3]$. Defining the $[a_1 \quad a_2 \quad a_3]$ vector as the cross product of $[u_1 \quad u_2 \quad u_3]$ and $[h_1 \quad h_2 \quad h_3]$ vectors and considering the$[b_1 \quad b_2 \quad b_3]$ vector to be the cross product of $[v_1 \quad v_2 \quad v_3]$ and $[l_1 \quad l_2 \quad l_3]$vectors, this rigid body rotation can be expressed as

$$(\gamma J\gamma) = \begin{pmatrix} u_1 & h_1 & a_1 \\ u_2 & h_2 & a_2 \\ u_3 & h_3 & a_3 \end{pmatrix} \begin{pmatrix} v_1 & l_1 & b_1 \\ v_2 & l_2 & b_2 \\ v_3 & l_3 & b_3 \end{pmatrix}^{-1}. \quad [10]$$

Therefore, the invariant line strain can be obtained as follows:

$$(\gamma S\gamma) = (\gamma J\gamma)\,(\gamma B\gamma). \quad [11]$$

Having determined the invariant line strain, $(\gamma S\gamma)$, it should be factorized according to the following equation for obtaining the shape deformation matrix, $(\gamma P\gamma)$.

$$(\gamma S\gamma) = (\gamma P\gamma)\,(\gamma Q\gamma), \quad [12]$$

where

$$(\gamma P\gamma) = \begin{pmatrix} 1 + md_1p_1 & md_1p_2 & md_1p_3 \\ md_2p_1 & 1 + md_2p_2 & md_2p_3 \\ md_3p_1 & md_3p_2 & 1 + md_3p_3 \end{pmatrix} \quad [13]$$

and

$$(\gamma Q\gamma) = \begin{pmatrix} 1 + ne_1q_1 & ne_1q_2 & ne_1q_3 \\ ne_2q_1 & 1 + ne_2q_2 & ne_2q_3 \\ ne_3q_1 & ne_3q_2 & 1 + ne_3q_3 \end{pmatrix}. \quad [14]$$

In Eq. [13], $[d_1 \quad d_2 \quad d_3]$ and $[p_1 \quad p_2 \quad p_3]$ are the unit vectors in the direction of macroscopic displacement and invariant plane normal of the transformation, respectively. m represents the magnitude of displacement due to the martensitic transformation. Since the lattice invariant shear has been assumed to occur on $(1 \quad 0 \quad 1)[\bar{1} \quad 0 \quad 1]$ system and because its effect is to cancel the shape change due to $(\gamma Q\gamma)$, according to the phenomenological theory of martensite phase transformation, the latter should be a shear on $(1 \quad 0 \quad 1)[1 \quad 0 \quad \bar{1}]$. Therefore, $[q_1 \quad q_2 \quad q_3]$ equals $[0.707 \quad 0 \quad 0.707]$ and $[e_1 \quad e_2 \quad e_3]$ can be expressed as $[0.707 \quad 0 \quad -0.0707]$. Since $(\gamma Q\gamma)$ should not change the volume, its determinant should be equal to unity.[18,19]

Rearranging Eq. [12], using Eqs. [13] and [14] and considering the indices of the vectors $[q_1 \quad q_2 \quad q_3]$ and $[e_1 \quad e_2 \quad e_3]$ results in

$$\begin{pmatrix} S_{11} & S_{12} & S_{13} \\ S_{21} & S_{22} & S_{23} \\ S_{31} & S_{32} & S_{33} \end{pmatrix} = \begin{pmatrix} 1 + md_1p_1 & md_1p_2 & md_1p_3 \\ md_2p_1 & 1 + md_2p_2 & md_2p_3 \\ md_3p_1 & md_3p_2 & 1 + md_3p_3 \end{pmatrix} \times \begin{pmatrix} 1 + n(0.707)^2 & 0 & n(0.707)^2 \\ 0 & 1 & 0 \\ -n(0.707)^2 & 0 & 1 - n(0.707)^2 \end{pmatrix}. \quad [15]$$

The following relations are obtained by multiplying each of the $(\gamma P\gamma)$ rows by the second column of $(\gamma Q\gamma)$, *i.e.*,

$$S_{12} = md_1p_2 \quad [16]$$

$$S_{22} = 1 + md_2p_2 \quad [17]$$

$$S_{32} = md_3p_2. \quad [18]$$

Since $(\gamma S\gamma)$ has been already calculated, each of the $(\gamma S\gamma)$ components are known. Dividing Eq. [16] by Eq. [18] gives

$$\frac{S_{12}}{S_{32}} = \frac{d_1}{d_3} \quad [19]$$

Or

$$d_3 = \frac{S_{32}}{S_{12}} d_1. \quad [20]$$

Equation [17] can be written as

$$md_2p_2 = S_{22} - 1. \quad [21]$$

Therefore,

$$\frac{S_{12}}{S_{22} - 1} = \frac{d_1}{d_2} \quad [22]$$

or

$$d_2 = \frac{S_{22} - 1}{S_{12}} d_1. \quad [23]$$

Since $[d_1 \quad d_2 \quad d_3]$ is a unit vector, the following relationship is obtained:

$$d_1^2 + d_2^2 + d_3^2 = 1. \quad [24]$$

Hence, the $[d_1 \quad d_2 \quad d_3]$ vector can be determined by solving Eqs. [20], [23], and [24] simultaneously.

The inverse of $(\gamma S\gamma)$ in Eq. [12] can be expressed as

$$(\gamma S\gamma)^{-1} = (\gamma Q\gamma)^{-1}(\gamma P\gamma)^{-1} \quad [25]$$

or

$$\begin{pmatrix} S_{11}^* & S_{12}^* & S_{13}^* \\ S_{21}^* & S_{22}^* & S_{23}^* \\ S_{31}^* & S_{32}^* & S_{33}^* \end{pmatrix} = \begin{pmatrix} 1-n(0.707)^2 & 0 & -n(0.707)^2 \\ 0 & 1 & 0 \\ n(0.707)^2 & 0 & 1+n(0.707)^2 \end{pmatrix} \times \begin{pmatrix} 1+md_3p_3+md_2p_2 & md_1p_1 & -md_1p_3 \\ md_2p_1 & 1+md_3p_3+md_1p_1 & md_2p_3 \\ -md_3p_1 & md_3p_2 & 1+md_2p_2+md_1p_1 \end{pmatrix} \frac{1}{\det(\gamma S\gamma)}. \quad [26]$$

It is worth noting that since $\det(\gamma Q\gamma) = 1$, $\det(\gamma P\gamma)$ is equal to $\det(\gamma S\gamma)$. It is clearly observable in Eq. [13] that

$$\det(\gamma P\gamma) = 1 + md_1p_1 + md_2p_2 + md_3p_3. \quad [27]$$

Multiplication of the second row of $(\gamma Q\gamma)^{-1}$ by each of the columns of $(\gamma P\gamma)^{-1}$ results in

$$S_{21}^* = \frac{md_2p_1}{\det(\gamma S\gamma)} \quad [28]$$

$$S_{22}^* = \frac{1 + md_3p_3 + md_1p_1}{\det(\gamma S\gamma)} \quad [29]$$

$$S_{23}^* = \frac{md_2p_3}{\det(\gamma S\gamma)}. \quad [30]$$

Since $(\gamma S\gamma)$ and $[d_1 \quad d_2 \quad d_3]$ have been already determined, S_{21}^*, S_{22}^*, S_{23}^*, d_1, d_2, d_3 , and $\det(\gamma S\gamma)$ are known. Therefore, $[mp_1 \quad mp_2 \quad mp_3]$ can be calculated by solving Eqs. [28], [29], and [30], simultaneously. Knowing that $[p_1 \quad p_2 \quad p_3]$ (normal of the habit plane) is a unit vector, the value of m is obtainable.

The values of α and R can be calculated by the following equations:

$$\alpha = [p_1 \quad p_2 \quad p_3] \begin{bmatrix} md_1 \\ md_2 \\ md_3 \end{bmatrix} \quad [31]$$

$$R = \left(m^2 - \alpha^2\right)^{1/2}. \quad [32]$$

α, R, and m, parameters together with the indices d_1, d_2, and d_3 in $[d_1 \quad d_2 \quad d_3]$ vector have been illustrated in Figure 1, schematically.

III. MATERIALS AND METHODS

The material investigated in this study was a TRIP800 steel sheet with the initial thickness of 1 mm. The chemical composition of the investigated steel is given in Table I.

X-ray diffraction experiments were carried out using Phillips X'pert diffractometer with Cuk$_\alpha$ radiation. The 2θ step size was equal to 0.02 deg and the exposure time

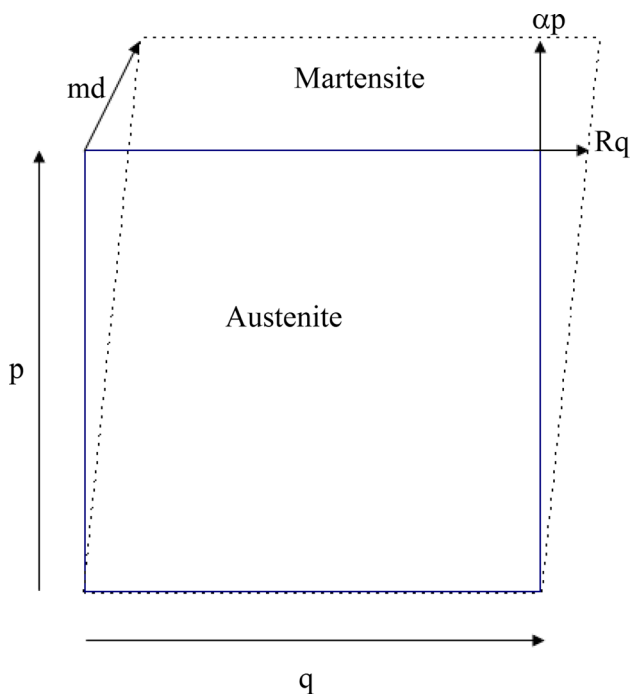

Fig. 1—Schematic representation of the most important parameters utilized in the crystallographic theory of martensitic phase transformation.

Table I. Chemical Composition of the Investigated Steel (in Wt. Percent)

Fe	C	Si	Mn	P	Al
Based	0.32	1.4	1.5	0.008	0.047

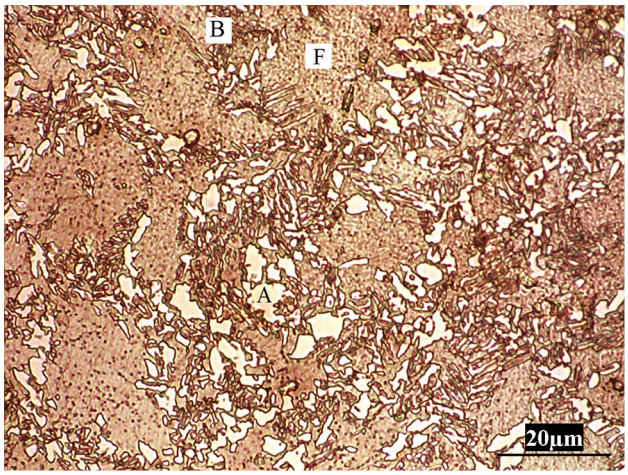

Fig. 2—Optical micrograph of the investigated TRIP800 steel. Illustrating the Bainite (B) and retained austenite (A) within the ferrite (F) matrix.

was 53 seconds during X-ray peak scanning. The samples were first mechanically polished and then, were chemically polished for 30 minutes using a 95pctH_2O_2-5pctHF solution,[21] before radiation exposure. The (111), (200), and (220) peaks of the austenite phase and (110), (200), and (211) peaks of the ferrite phase were chosen for subsequent analyses.

Specimens for optical metallography were polished following a detailed procedure recommended by Buehler Ltd.,[22] and then, were etched in a solution prepared by adding 10 g sodium metabisulfite into 100 ml water.[23] Tensile specimens 25 mm in length and 6 mm in width were cut from the steel sheet by wire electro-discharge machining to avoid strain-induced martensitic transformation during sample preparation. Tensile test was conducted using a screw-driven Zwick Z250 universal tensile testing machine at a constant cross head speed of 10 mm/min corresponding to an initial strain rate of 6.67×10^{-3} s^{-1}.

IV. FINITE ELEMENT ANALYSIS

The finite element model using the real microstructure of the low alloy TRIP800 steel[13–15] was employed in this study. The optical micrograph of the investigated steel (Figure 2) was used for the subsequent image processing and imported into the ABAQUS general purpose commercial finite element code.[24] It needs to be mentioned that the volume fraction and morphology of the constituent phases in Figure 2, which has been chosen to be the representative volume element, are almost equal to the corresponding average values for the whole steel microstructure measured by the image analysis software. Since tensile specimens have been cut from the steel sheet and these specimens undergo an in-plane loading condition during both uniaxial and biaxial tensile tests, two-dimensional three-node plane stress element (CPS3) were adopted for discretization of the representative volume element. In the discretized micrograph illustrated in Figure 3, the phase boundaries were explicitly modeled with a finer mesh for the subsequent study of failure initiation.

In the simulation of the uniaxial tensile loading, the same displacement was applied on the nodes located along the right edge of the representative volume element in the x direction, while these nodes could move freely in the y direction. The nodes located in the left edge of the representative volume element were considered to be fixed in x direction, but allowed to move freely in the y direction. Since the representative volume element should remain rectangular during deformation, the top and bottom edges of the element were constrained so that all the nodes located along these edges displace the same in the y direction. For modeling the biaxial tensile deformation, the nodes located along the left and bottom edges of the representative volume element were considered not to move in the x and y directions, respectively; while the right and top edges of the element were subjected to displacements along the respective x and y directions based on the corresponding principal strain ratio, $\varepsilon_{22}/\varepsilon_{11}$. In the case of equibiaxial deformation, for example, the right and top edges of the element were displaced in the respective x and y directions so that the element experiences the same strain along x and y directions. Macroscopic engineering stresses were obtained by dividing the reaction forces of the right and top edges of the volume element in the respective x and y directions by the corresponding initial length. Macroscopic engineering strains were also calculated by dividing the right and top edge displacements by the initial length of the respective horizontal and vertical edges of the representative volume element.

In the current work, all the constituent phases of the TRIP steel were assumed to have isotropic elastic–plastic deformation behavior. The Young's modulus and Poisson's ratio of the constituent phases were considered to be 210 GPa and 0.3, respectively.[13–15] The flow stresses of ferrite and bainite phases were assumed to follow the so-called Ludwik–Hollomon equation (Eq. [33]), while the Swift equation (Eq. [34]) was adopted for predicting the flow curves of retained austenite and martensite phases. The flow behavior of retained austenite and martensite in the TRIP800 steel with the chemical composition as that utilized in the current work has been reported to be estimated by the Swift law.[25] Since ferrite and bainite phases have not been distinguished from each other in Reference 25, the reported value for the flow stress of the ferrite in this

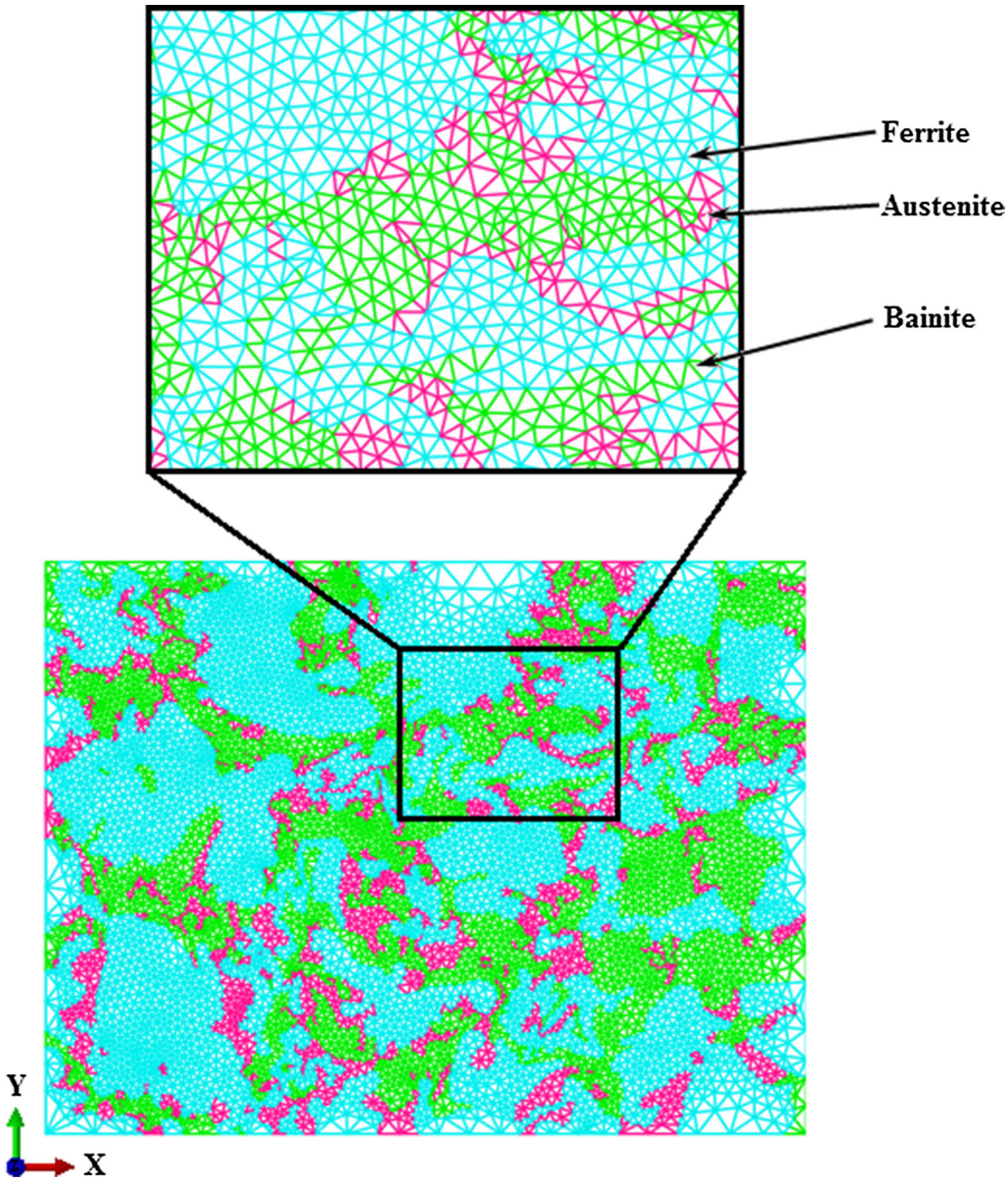

Fig. 3—The discretized representative volume element (RVE).

reference cannot be used in this study. Instead, the values employed for the prediction of flow stress as a function of plastic strain in other related references have been adopted for the purpose of simulations in this work.[15] Since the chemical compositions of ferrite phase in all low alloy TRIP steels are almost similar,[26] and this is the case for bainite phase as well, the flow behavior of these phases has been assumed to be almost the same as those reported in the literature for low alloy TRIP steels. The following well-known equations were assumed for constituent phases of the investigated TRIP steel samples in the present study.

$$\sigma_i = \sigma_{y,i} + K_i \varepsilon_{\text{ep}}^{n_i} \quad (i = F, B) \qquad [33]$$

$$\sigma_{y,i} = \sigma_{\text{yo},i}(1 + H_{o,i}\varepsilon_{\text{ep}})^{n_i} \quad (i = A, M). \qquad [34]$$

All the parameters in Eqs. [33] and [34] which are obtained from the literature are given in Table II.

The kinetics of strain-induced martensitic transformation expressed by Eq. [1] was implemented into ABAQUS general purpose finite element code using a user material subroutine (UMAT). In this subroutine, the current magnitude of the mechanical driving force for martensitic transformation in each integration point of the elements belonging to the austenite phase is compared with the critical value of the mechanical driving force for the transformation. It is assumed that strain-induced martensitic transformation occurs when the current mechanical driving force exceeds the critical value. In this case, the mechanical properties of the integration point change to those of the martensite phase.

Table II. Values of the Material Parameters

Ferrite	
E (GPa)	210
v	0.3
K	1200
σ_y (MPa)	425
n	0.6
Bainite	
E (GPa)	210
v	0.3
K	3400
σ_y (MPa)	500
n	0.65
Austenite	
E (GPa)	210
v	0.3
σ_{y0}	700
H_0	50
n	0.24
Martensite	
E (GPa)	210
v	0.3
σ_{y0}	2300
H_0	100
n	0.05

V. RESULTS AND DISCUSSIONS

The X-ray diffraction patterns of the investigated steel in both the as-received and uniaxially deformed state (fractured) are shown in Figure 4. As it is clearly seen in Figure 4, the as-received sample contains two different phases, *i.e.*, the body-centered cubic (BCC) ferrite (α) phase and the face-centered cubic (FCC) austenite (γ) phase. After uniaxial deformation, all of the diffraction peaks for γ phase except for the peak corresponding to (111) plane disappear indicating that the strain-induced martensitic transformation has occurred.

The average lattice parameters of the austenite and ferrite phases can be determined by the average diffracting angles, $2\theta_i$, which are obtained from XRD experiments corresponding to each $\{h \quad k \quad l\}$ plane, using the following relation[27]:

$$a = \frac{1}{N}\sum_{i=1}^{N}\left(\frac{\lambda}{2}\right)\frac{\sqrt{h^2+k^2+l^2}}{\sin(\theta_i)}. \qquad [35]$$

In this equation, N is the number of reflection and λ is the incident X-ray beam wavelength. The carbon content (in weight percent) of the austenite phase, C_γ, can be estimated by the following equation[21,28]:

$$a_\gamma = 0.35467 + 0.00467C_\gamma\,(\text{nm}), \qquad [36]$$

where a_γ is the austenite lattice parameter.

In martensitic phase transformation, the austenite phase transforms into martensite (α') with body-centered tetragonal (BCT) crystal structure. The martensite lattice parameters are related to the average carbon content of the parent austenite phase through the following empirical equations[27]:

$$a_{\alpha'} = a_\alpha - 0.0014C_\gamma\,(\text{nm}) \qquad [37]$$

$$c_{\alpha'} = a_\alpha + 0.0115C_\gamma\,(\text{nm}),$$

where $a_{\alpha'}$ and $c_{\alpha'}$ are the lattice parameters of the martensite phase and a_α is the lattice parameter of the ferrite phase.

The volume fraction of retained austenite can be obtained from the relative intensities of multiple diffraction peaks using the following equation[29]:

$$V_\gamma = \frac{\frac{1}{q}\sum_{j=1}^{q}\frac{I_{\gamma j}}{R'_{\gamma j}}}{\frac{1}{p}\sum_{i=1}^{p}\frac{I_{\alpha i}}{R'_{\alpha i}}+\frac{1}{q}\sum_{j=1}^{q}\frac{I_{\gamma j}}{R'_{\gamma j}}}, \qquad [38]$$

where V_γ is the austenite volume fraction; $I_{\alpha i}$ and $I_{\gamma j}$ are the integrated intensities corresponding to the ith and jth peaks of the respective ferrite and austenite phases. p and q are the number of the respective ferrite and austenite diffraction peaks which has been chosen for the calculation.

The value of R' parameter corresponding to each of the constituent phases can be expressed as follows[29,30]:

$$R' = \left(\frac{1}{v^2}\right)\left[|F|^2 p\left(\frac{1+\cos^2 2\theta}{\text{Sin}^2\theta\text{Cos}\theta}\right)\right]e^{-2\text{M}}, \qquad [39]$$

where v is the volume of unit cell, F the structural factor, p the multiplicity factor, θ the Bragg angle, and $e^{-2\text{M}}$ denotes the temperature factor. As mentioned before, the (111), (200), and (220) peaks of austenite and those of (110), (200), and (211) planes for ferrite were chosen for the calculation of V_γ.

The average lattice parameters of the constituent phases together with the average carbon content and volume fraction of retained austenite in the as-received state were estimated by both XRD results and those of image analysis, and the results are listed in Table III.

Using the estimated lattice parameters of the austenite and martensite phases, the Bain strain, habit plane, shape deformation matrix, and R and α parameters of martensitic phase transformation were calculated based on the corresponding formulae mentioned before. These calculated values are given in the following:

$$(\gamma B\gamma) = \begin{pmatrix} 1.11786 & 0 & 0 \\ 0 & 1.11786 & 0 \\ 0 & 0 & 0.832454 \end{pmatrix}, \qquad [40]$$

$$\text{Habit plane} : (-0.17724 \quad -0.80657 \quad -0.65394), \qquad [41]$$

$$(\gamma B\gamma) = \begin{pmatrix} 0.9935 & -0.0298 & -0.0208 \\ 0.0249 & 1.1133 & 0.07902 \\ -0.0209 & -0.0953 & 0.9334 \end{pmatrix}, \qquad [42]$$

$$R = 0.18, \qquad [43]$$

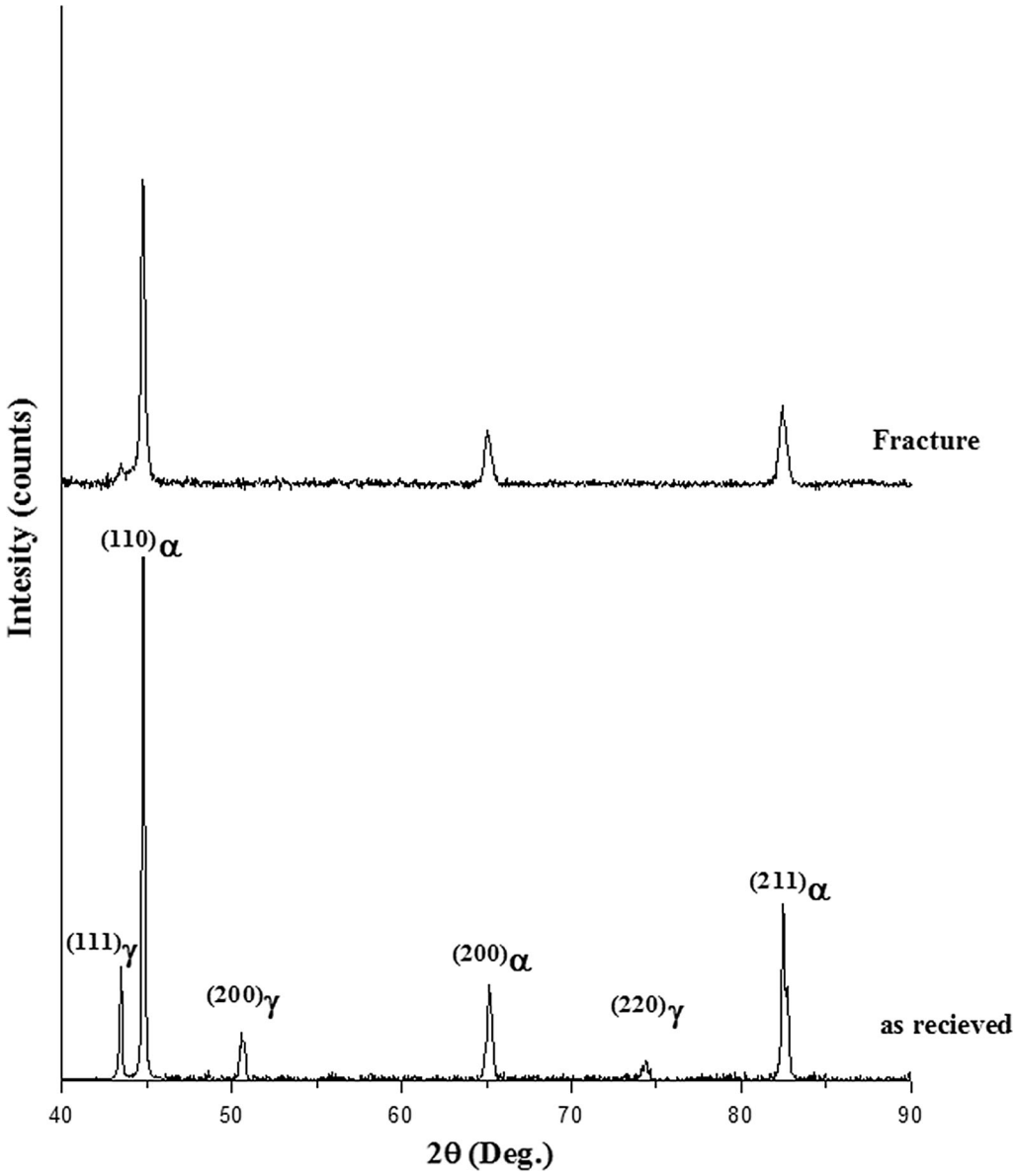

Fig. 4—X-ray diffraction patterns of microstructure of the as-received and uniaxially deformed state (fractured) TRIP800 steel.

$$\alpha = 0.04. \quad [44]$$

The values of R and α parameters calculated for martensitic transformation of the investigated steel are in good agreement with those reported in the literature for the same material.[31]

In the current work, the critical mechanical driving force of the martensitic transformation has been assumed to be the same as the thermodynamic free energy change for this transformation per unit volume. The thermodynamic free energy change of the martensitic phase transformation at the martensite start temperature has been reported to be estimated by the following expression[32]:

$$\Delta G^{\gamma\to\alpha'} = 2x\mathrm{RT}\ln x + x\left|\Delta\bar{H}_c^{\alpha} - \Delta\bar{H}_c^{\gamma} - \left(\Delta\bar{S}_{xs}^{\alpha} - \Delta\bar{S}_{xs}^{\gamma}\right)T + 4\omega_{\alpha} - 6\omega_{\gamma}\right| + A, \quad [45]$$

where

$$A = -4\mathrm{RT}(1-x)\ln(1-x) + 5\mathrm{RT}(1-2x)\ln(1-2x) - 6\mathrm{RT}x\ln\left|\frac{\delta_{\gamma}-1+3x}{\delta_{\gamma}+1-3x}\right| + B \quad [46]$$

$$B = -6\mathrm{RT}(1-x)\ln\left|\frac{1-2J_{\gamma}+(4J_{\gamma}-1)x-\delta_{\gamma}}{2J_{\gamma}(2x-1)}\right| + 3\mathrm{RT}x\ln(3-4x) + C \quad [47]$$

Table III. The Lattice Parameters of Different Phases (α: Ferrite, γ: Austenite and α′: Martensite) and the Volume Fraction and Carbon Content of Retained Austenite in the Investigated Steel

Volume Fraction of Retained Austenite (Pct)		a_γ (nm)	a_α (nm)	C_γ (Wt Pct)	$a_{\alpha'}$ (nm)	$c_{\alpha'}$ (nm)
X-ray diffraction	Image analysis	0.36014	0.286315	1.18	0.28467	0.2998
18	17.8					

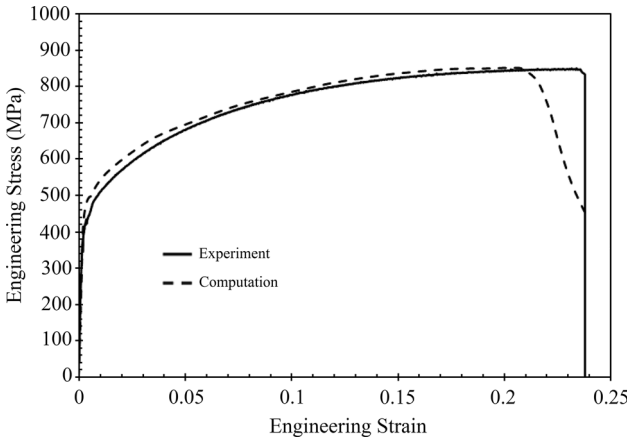

Fig. 5—Engineering stress-engineering strain curves of the studied TRIP800 steel.

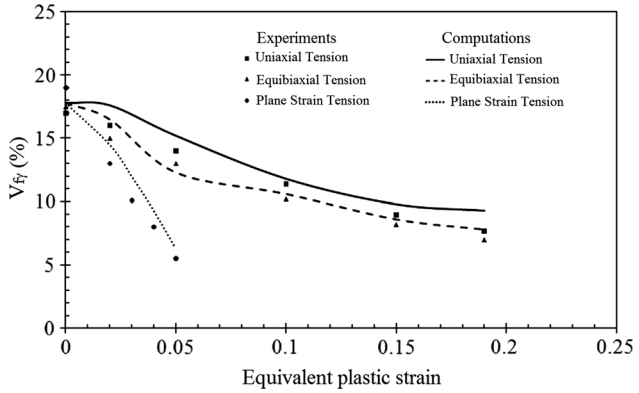

Fig. 6—Variation of the volume fraction of retained austenite as a function of applied strain under different loading conditions.

$$C = 4\mathrm{RT}x\ln\left|\frac{\delta_\alpha - 3 + 5x}{\delta_\alpha + 3 - 5x}\right| + (1-x)\Delta G_{Fe}^{\gamma\to\alpha} + \Delta f^*. \quad [48]$$

In these equations, x is the mole fraction of carbon in the austenite phase, T refers to the martensite start temperature, R is the universal gas constant, $\Delta\bar{H}_c^\alpha = 111918\,\mathrm{J/mol}$, $\Delta\bar{S}_{xc}^\alpha = 51.44\,\mathrm{J/molK}$, and

$$\Delta\bar{H}_c^\gamma = 35129 + 169105x \quad \mathrm{J/mol} \quad [49]$$

$$\Delta\bar{S}_{xs}^\gamma = 7.639 + 120.4x \quad \mathrm{J/molK} \quad [50]$$

$$\delta_\alpha = \left|9 - 6x(2J_\alpha + 3) + (9 + 16J_\alpha)x^2\right|^{1/2} \quad [51]$$

$$\delta_\gamma = \left|1 - 2x(1 + 2J_\gamma) + (1 + 8J_\gamma)x^2\right|^{1/2} \quad [52]$$

$$J_\alpha = 1 - \exp\left(-\frac{\omega_\alpha}{\mathrm{RT}}\right) \quad [53]$$

$$J_\gamma = 1 - \exp\left(-\frac{\omega_\gamma}{\mathrm{RT}}\right) \quad [54]$$

$$\omega_\alpha = 48570\,\mathrm{J/mol} \quad [55]$$

$$\omega_\gamma = 8054\,\mathrm{J/mol}. \quad [56]$$

Considering the estimated carbon content of retained austenite, the mole fraction of carbon in this phase is estimated to be 0.052 and hence, the martensite start temperature of the studied steel will be estimated to be around 400 K (127 °C).[33] The values of $\Delta G^{\gamma\to\alpha}$ and Δf^* have been obtained from the relevant References 34, 35. Therefore, the critical driving force for the martensitic phase transformation in the investigated steel can be calculated as 1330 J/mol. Dividing this value by the molar volume of austenite phase, results in the estimated critical driving force, *i.e.*, 190 MPa, for martensitic transformation in the investigated steel. It is worth mentioning that the molar volume of austenite can be obtained from the estimated lattice parameter of this phase.

Experimentally determined variation of the retained austenite volume fraction as a function of applied strain shows that the maximum transformation rate occurs during plane strain tension, and the transformation rate during uniaxial tension is lower than that when the steel deforms in equibiaxial tension.[31] The value of stress state sensitivity parameter of martensitic transformation, k, was determined so that the above-mentioned transformation rate trend was obtained numerically. This value was found to be 0.15.

Figure 5 shows the engineering stress–strain curve of the investigated steel predicted by the utilized microstructure-based finite element method together with the experimental data obtained by the uniaxial tensile test. As can be observed, there is a good

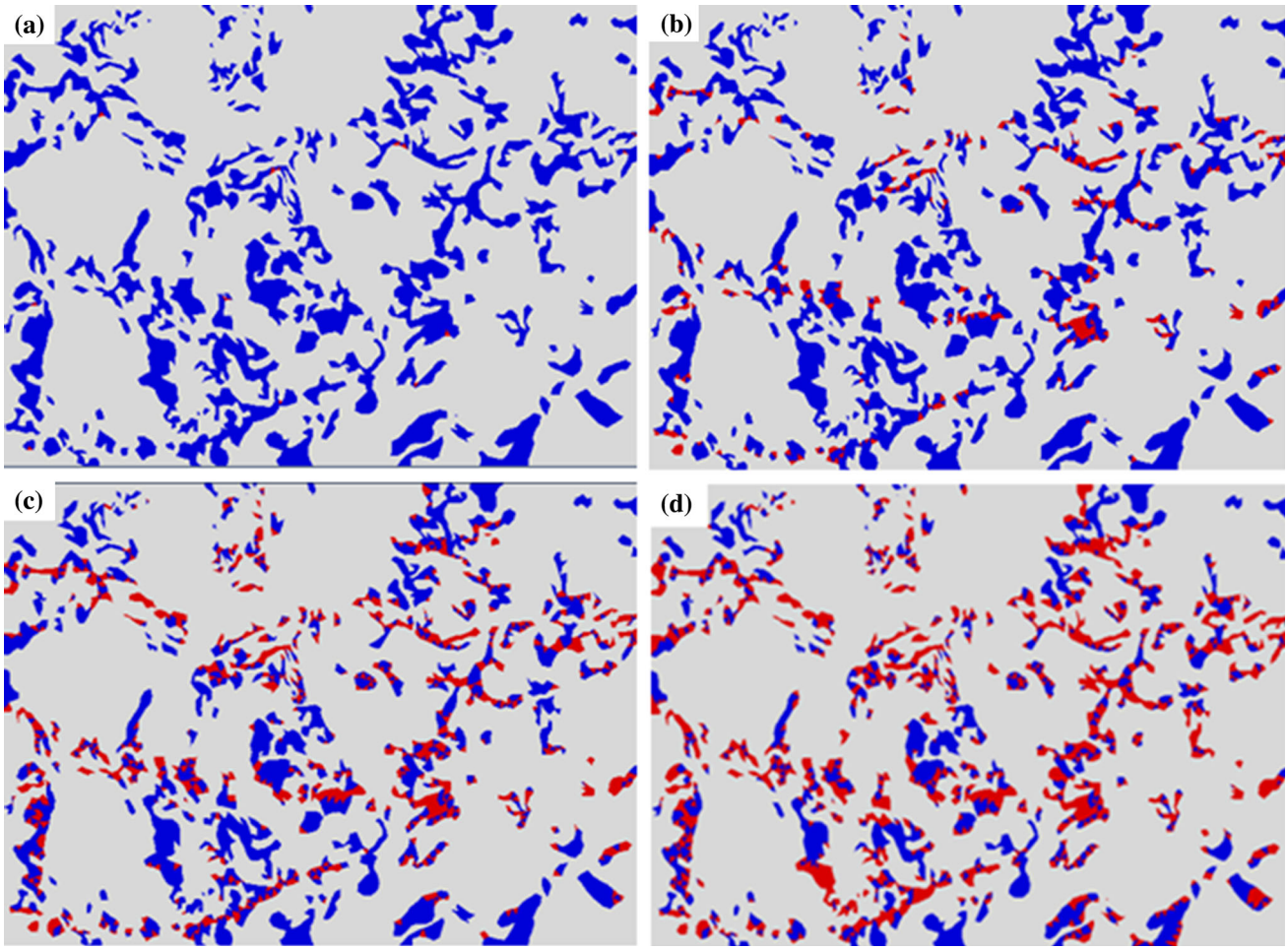

Fig. 7—Martensite volume fraction evolution in the RVE under uniaxial tension at various engineering strains of (*a*) 2 pct, (*b*) 5 pct, (*c*) 10 pct, and (*d*) 15 pct.

agreement between the experimental and predicted results. Particularly, the employed numerical method is capable of estimating the ultimate tensile strength (UTS), the engineering strain corresponding to UTS, and the engineering failure strain satisfactorily.

The volume fraction of retained austenite as a function of equivalent strain of the representative volume element under different loading conditions estimated by the utilized microstructure-based finite element method is given in Figure 6. The experimentally determined volume fraction of retained austenite as a function of equivalent strain obtained under the same loading conditions as those used in numerical estimation, extracted from the literature, is also superimposed on Figure 6. As it is clearly observable in this figure, there is an appropriate correlation between the numerical and experimental results.

It should be mentioned that the variation of martensite volume fraction in the representative volume element has been estimated by image analysis. For example, the evolution of martensite phase in the representative volume element under uniaxial tension is shown in Figure 7. In this figure, the red and blue areas represent the martensite and retained austenite phases, respectively. The remaining part of the microstructure is shown as white regions. The volume fraction of martensite and/or retained austenite phase can be estimated by the analysis of these digitized images using the same procedure as that used for determining volume fraction of a phase in a particular micrograph.

From Figures 5 and 6, it is clear that although the mechanical behavior of constituent phases used in the current work has not been obtained by *in situ* techniques and all the parameters describing the martensitic transformation kinetics except the sensitivity of transformation to the stress state have been estimated theoretically, the numerical method used in this work has a good capability for predicting both the mechanical properties and martensitic transformation kinetics of the TRIP800 steel.

Figure 8 (part a to part e) shows the equivalent plastic strain distribution in the representative volume element of the investigated material deformed in uniaxial tension at different engineering strains. As it can be clearly seen in this figure, with an increase in the applied strain, the plastic strain localization increases within the representative volume element. The equivalent plastic strain

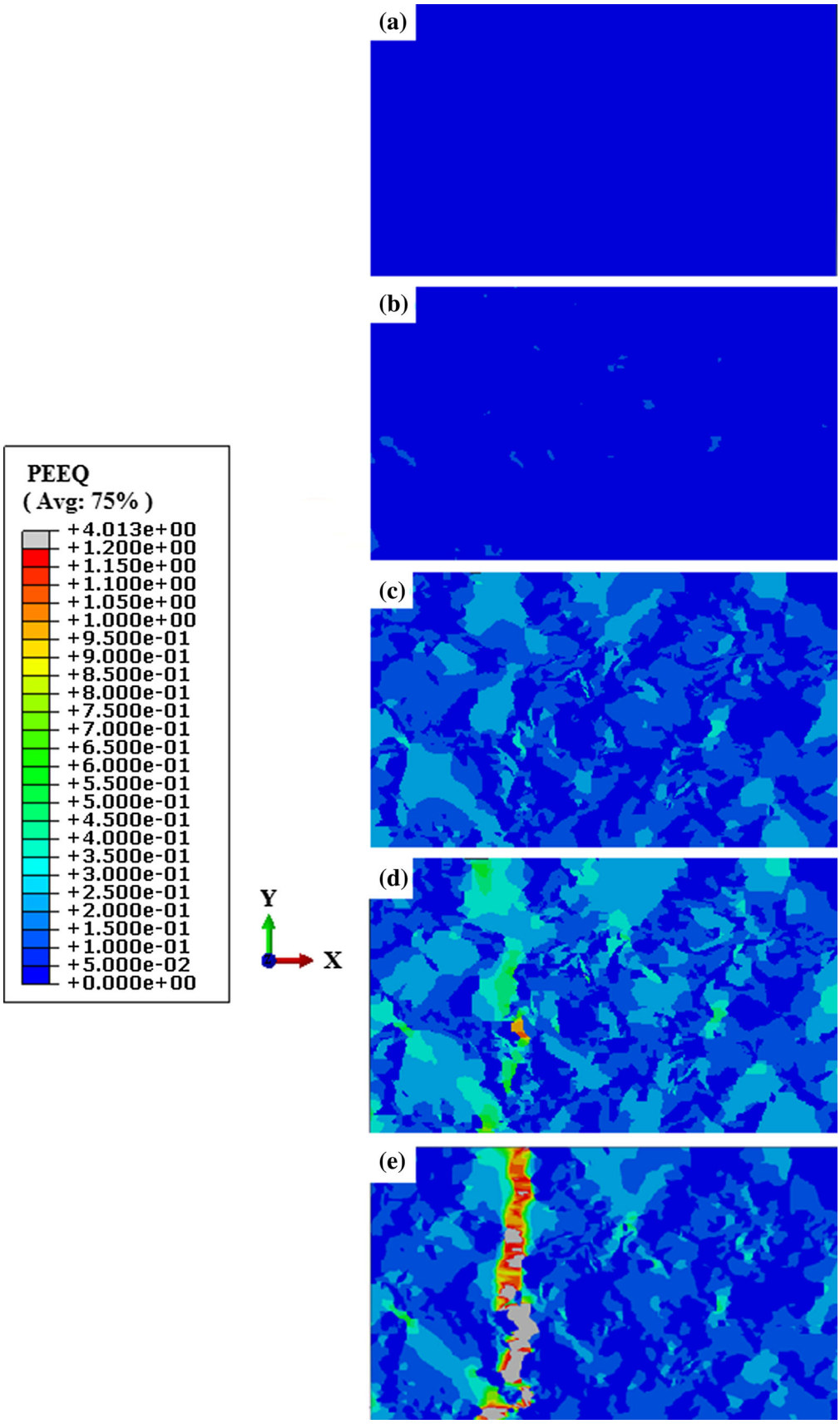

Fig. 8—Distribution of equivalent plastic strain for TRIP800 steel at various engineering strains of (*a*) 2 pct, (*b*) 5 pct, (*c*) 15 pct, (*d*) 20.6 pct, and (*e*) 24 pct.

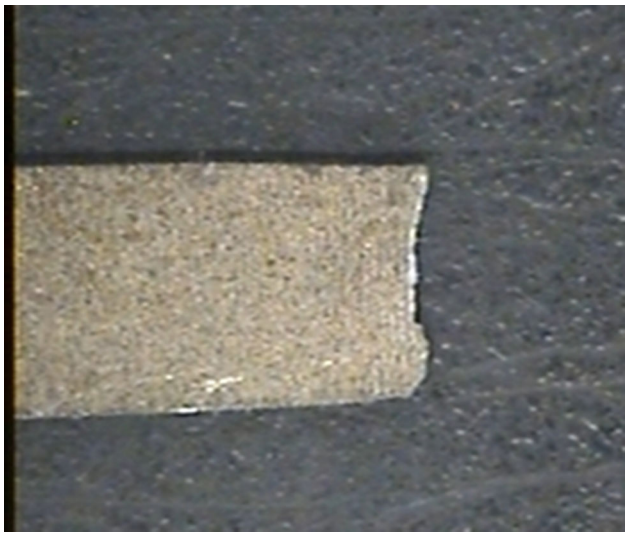

Fig. 9—A failed tensile specimen of TRIP800 steel.

distribution at the applied strain value corresponding to the failure strain clearly shows that the equivalent plastic strain has been localized at a narrow band in a situation approximately perpendicular to the loading direction. Therefore, it can be said that the failure phenomenon in the material during deformation in uniaxial tension has most probably occurred by plastic strain localization perpendicular to the loading direction.

The fractured tensile specimen is shown in Figure 8. In this figure, the loading direction is the same as that of the assumed representative volume element which has been used in the numerical calculation. As can be observed in this figure, the fracture surface of the tensile specimen is almost flat and perpendicular to the loading direction. The shape and relative orientation of the fractured region is almost the same as the equivalent plastic strain localization band in the representative volume element predicted by the numerical method (Figure 8(e)). This is an additional reason for the fact that fracture in this specimen has taken place by plastic strain localization perpendicular to the loading direction.

Figures 8 and 9 show that the microstructure-based finite element model used in this research work can predict ductility and failure mode of TRIP800 steel (at least during uniaxial tension) with an acceptable accuracy.

VI. SUMMARY AND CONCLUSION

The finite element model based on the actual microstructure was used to predict uniaxial engineering stress-engineering strain curve of TRIP800 steel as well as the variation of martensite volume fraction in its microstructure as a function of the applied strain under different loading conditions. The martensitic transformation kinetics was predicted by the use of a computational model which has already been developed. Dilational (α) and shear (R) strains generated in the steel due to martensitic transformation needed to be used in the transformation kinetics model were estimated using the crystallographic theory of the martensitic transformation.

In this study, the critical mechanical driving force of the martensitic transformation was assumed to be the same as thermodynamic free energy change of the transformation per unit volume and the amount of this critical value was estimated to be 190 MPa for the investigated steel. The value of the stress state sensitivity parameter of the martensitic transformation, k, *i.e.*, 0.15, was determined so that the variation of martensite volume fraction during different loading conditions was successfully predicted by the numerical method. The mechanical behavior of each constituent phase was extracted from the literature and the utilized martensitic transformation kinetics was implemented into ABAQUS general purpose finite element code by a user material subroutine. The results of finite element simulation under different loading conditions showed that a good agreement exists between both the mechanical and transformation behaviors of the investigated TRIP800 steel. Moreover, using this microstructure-based finite element method ductility and failure mode of the investigated steel during uniaxial tension were predicted and it was found that there is an appropriate correlation between the experimental and predicted results.

ACKNOWLEDGMENT

The authors wish to thank Prof. W.J. Poole at university of British Columbia for providing the TRIP steel for this study.

REFERENCES

1. O. Muransky, P. Hornak, P. Lukas, J. Zrnik, and P. Sittner: *J. Ach. Mater. Manuf. Eng.*, 2006, vol. 14, pp. 26–30.
2. G.B. Olson and M. Cohen: *Metall. Trans. A*, 1975, vol. 6, pp. 791–95.
3. R.G. Stringfellow, D.M. Parks, and G.B. Olson: *Acta Metall. Mater.*, 1992, vol. 40, pp. 1703–16.
4. T. Iwamoto, T. Tsuta, and Y. Tomita: *Int. J. Mech. Sci.*, 1998, vol. 16, pp. 173–82.
5. T. Iwamoto and T. Tsuta: *Int. J. Plast.*, 2000, vol. 16, pp. 791–804.
6. I. Papatriantafillou, N. Aravas, and G.N. Haidemenopoulos: *Steel Res. Int.*, 2004, vol. 75, pp. 730–36.
7. T. Iwamoto: *Int. J. Plast.*, 2004, vol. 20, pp. 841–69.
8. A. Perlade, O. Bouaziz, and Q. Furnémont: *Mater. Sci. Eng. A*, 2003, vol. 356, pp. 145–52.
9. F. Marketz and F.D. Fischer: *Comput. Mater. Sci.*, 1994, vol. 3, pp. 307–25.
10. G. Reisner, E.A. Werner, and F.D. Fischer: *Int. J. Solids Struct.*, 1998, vol. 35, pp. 2457–73.
11. L. Taleb and F. Sidoroff: *Int. J. Plast.*, 2003, vol. 19, pp. 1821–42.
12. H.N. Han, C.G. Lee, C.S. Oh, T.H. Lee, and S.J. Kim: *Acta Mater.*, 2004, vol. 52, pp. 5203–14.
13. K.S. Choi, W.N. Liu, X. Sun, M.A. Khaleel, Y. Ren, and Y.D. Wang: *Metal. Mater. Trans. A*, 2008, vol. 39, pp. 3089–96.
14. K.S. Choi, W.N. Liu, X. Sun, and M.A. Khaleel: *Acta Mater.*, 2009, vol. 57, pp. 2592–2604.
15. K.S. Choi, A. Solami, W.N. Liu, X. Sun, and M.A. Khaleel: *Comput. Mater. Sci.*, 2010, vol. 50, pp. 720–30.

16. M. Cherkaoui, A. Soulami, A. Zeghloul, and M.A. Khaleel: *Phil. Mag*., 2010, vol. 88, pp. 3479–3512.
17. J. Serri and M. Cherkaoui: *J. Eng. Mater. Technol*., 2008, vol. 130, pp. 1–13.
18. H.K.D.H. Bhadeshia: *Geometry of crystals*, 2nd ed., Fellow of Darwin College, Cambridge, 2006.
19. S. Kundu, Ph. D. Thesis, University of Cambridge, 2007.
20. J.W. Christian: *The theory of transformation in metals and alloys*, Pergamon, New York, 2002.
21. C. M. Parish, M. Sc. Thesis, University of Pittsburgh, Pennsylvania, 2003.
22. G.F. Vander Voort: *Metallography; Principles and Practice, Materials and Engineering Series*, McGraw-Hill, New York, 1984.
23. M. Mazinani, Ph. D. Thesis, University of British Columbia, Vancouver, BC, 2006.
24. ABAQUS general purpose finite element program, Version 6-10-1, Dassault Systemes Simulia Corp., Providence, 2010.
25. L. Delannay, P. Jacques, and T. Pardoen: *Int. J. Solids Struct*., 2008, vol. 45, pp. 1825–43.
26. H.K.D.H. Bhadesia and D.V. Edmonds: *Metall. Trans A*, 1979, vol. 10, pp. 895–907.
27. N.H. van Dijk, A.M. Butt, L. Zhao, J. Sietsma, S.E. Offerman, J.P. Wright, and S. van der Zwaag: *Acta Mater*., 2005, vol. 53, pp. 5439–47.
28. M.Y. Zhang, F.X. Zhu, and D.S. Zheng: *Int. J. Iron Steel Res*., 2011, vol. 18, pp. 73–78.
29. E975-03, Standard practice for X-ray determination of retained austenite in steel with near random crystallographic orientation, 2003.
30. B.D. Cullity: *Elements of X-ray Diffraction*, Addison-Wesley publishing Co. Inc, Reading, 1978, vol. 2.
31. P.J. Jacques, Q. Furnemont, F. Lani, T. Pardoen, and F. Delannay: *Acta Mater*., 2007, vol. 55, pp. 3681–93.
32. H.K.D.H. Bhadeshia: *Metal. Sci*., 1981, vol. 15, pp. 175–77.
33. S. Li, R. Zhu, I. Karaman, and R. Arroyave: *Acta Mater*, 2012, vol. 60, pp. 6120–30.
34. J.A. Lobo and G.H. Geiger: *Metall. Trans A*, 1976, vol. 7, pp. 1347–57.
35. J.C. Fhisher: *Met. Trans*, 1949, vol. 185, pp. 688–90.